Turkish Journal of Physics

http://journals.tubitak.gov.tr/physics/

Research Article

Turk J Phys
(2015) 39: 272 – 279

doi:10.3906/fiz-1504-6

A comparative study: synthetic dyes as photosensitizers for dye-sensitized solar cells

Amal M. AL-KAHLOUT[1], Hatem S. EL-GHAMRI[2,3], Naji Al DAHOUDI[1], Taher M. EL-AGEZ[2,3], Sofyan A. TAYA[2,3,*], Monzir S. ABDEL-LATIF[3,4]

[1]Department of Physics, Al Azhar University, Gaza, Palestinian Authority
[2]Department of Physics, Islamic University of Gaza, Gaza, Palestinian Authority
[3]Renewable Energy Center, Islamic University of Gaza, Gaza, Palestinian Authority
[4]Department of Chemistry, Islamic University of Gaza, Gaza, Palestinian Authority

Received: 15.04.2015 • **Accepted/Published Online:** 01.09.2015 • **Printed:** 30.11.2015

Abstract: In this paper, dye-sensitized solar cells (DSSCs) were fabricated using a zinc oxide (ZnO) semiconducting layer and different synthetic dyes. Eight different synthetic dyes were used to fabricate the DSSCs. Nanocrystalline ZnO powder was coated on transparent conducting fluorine-doped tin oxide glass using the doctor blade method to form a thin layer. The absorption spectra of the synthetic dyes were investigated. DSSCs were characterized with J-V characteristic curves. The parameters reflecting the cell performance were calculated. The results revealed that eosin Y dye corresponds to the highest conversion efficiency. The dependence of the sintering temperature and the thicknesses of the ZnO layer on the performance of the cell was investigated.

Key words: Dye-sensitized solar cell, synthetic dyes, ZnO

1. Introduction

Dye-sensitized solar cells (DSSCs) are among the most promising organic solar cells. Since their invention by O'Regan and Grätzel in 1991 [1], they have received great attention in the scientific community. A conversion efficiency of 10.8% was reported for a DSSC fabricated using TiO_2 nanopowder as a semiconducting material [2]. DSSCs have been known as one of the types of third-generation solar cells [3]. The principle of operation of a DSSC is based on the photosensitization of wide band-gap semiconductors using a proper chemical or natural dye. This photosensitization occurs when the dye absorbs part of the visible light spectrum and injects the excited electron into the conduction band of the semiconductor. DSSCs have been extensively studied by many physicists and engineers due to their unique advantages such as low cost [4–14]. DSSCs based on TiO_2 have been intensively investigated [4–6]. ZnO has many features such as its band gap, electron affinity, and electron injection efficiency. These features enable ZnO to be an alternative photoelectrode in DSSCs. Recently, ZnO has been widely investigated as a DSSC photoelectrode [7–9,15]. Compared to DSSCs based on TiO_2, the efficiencies of ZnO-based cells are still low. ZnO-based cells have reached efficiencies in the 5% range [16].

Versatility of BODIPY (4,4-difluoro-4-bora-3a,4a-diaza-s-indacene) dyes was expanded in recent DSSC applications [17]. A series of derivatives designed to address earlier problems in BODIPY sensitized solar cells was reported. ZnO nanorod structured DSSCs were fabricated and characterized [18].

*Correspondence: staya@iugaza.edu.ps

In this work, ZnO nanopowder was used as a photoelectrode of DSSCs. The fabricated cells were dyed with different synthetic dyes. ZnO paste was spread on transparent conducting fluorine-doped tin oxide (FTO) coated glass using the doctor blade method. The absorption spectra of chemical dyes were conducted in the spectral range from 300 to 800 nm. The $J-V$ characteristic curves of the DSSCs were measured and studied. The photovoltaic parameters of the fabricated cells were determined. The performance of the fabricated cells was studied with the sintering temperature and thickness of the ZnO layer.

2. Experimental and characterization

2.1. ZnO powder preparation and characterization

ZnO nanoparticles were prepared at pH 12 by dissolving 2.2 g of zinc acetate dihydrate, reagent $Zn(CH_3COO)_2 2.2 H_2O$, in 50 mL of methanol. After stirring for 12 h, a 0.2 M solution was prepared [19]. The preparation technique details can be found elsewhere [19,20]. The powder was then crushed using a hammer to diminish the size of the agglomerates. Finally, a fine powder was obtained.

A Bruker AXS D8 unit was used to study the crystalline structure of the prepared powder using Cu Kα radiation of wavelength 0.154 nm. The unit was operated at 40 kV and 40 mA. A highly sensitive detector (LynxEye) was utilized to record the diffracted intensity. The scanning process was conducted at $2\theta = 10^\circ$ to 100°. The TOPAS program was employed for the diffraction pattern analysis. The Scherrer equation was used to calculate the mean crystallite size of the ZnO powder. The obtained diffraction pattern is plotted in Figure 1. As can be seen from the figure, the powder has high crystallinity. Moreover, the structure corresponds to the typical wurtzite hexagonal structure (JCPDS No. 0036–1451 WL 15406 Hexagonal-03 24982). The crystallite mean value was obtained (12 nm). Peaks (101) and (002) were employed to find the crystallite size. For the (101) and (002) peaks, the crystallite sizes were found to be 12 nm and 11 nm, respectively. The dimensions a, b, and c of the lattice were also obtained [a = b = 3.253(0) Å, and c = 5.213(4) Å].

Surface morphology (SM) and Brunauer–Emmett–Teller (BET) surface area are considered two crucial parameters for DSSC application. The SM and the ZnO nanoparticle sizes were examined by scanning electron microscopy (JSM67500F, JEOL). The secondary electron signal excited by a 10 keV primary beam at an operating potential of 15 kV was used. Transmission electron microscopy (HRTEM-CM200 FEG, Philips) operated at 200 kV was employed to determine the morphology of the ZnO nanoparticles and the particle size.

The BET surface area was found to be 42.3 $m^2\ g^{-1}$. When compared to the BET obtained by Aghababazadeh et al. [21], which was 23.8 $m^2\ g^{-1}$, the value obtained in the current work is much higher. The low value of the BET obtained by Aghababazadeh et al. can be attributed to agglomeration of the particles during the sintering process. The agglomeration of the nanoparticles significantly reduces the surface area. A SEM picture for the prepared ZnO nanopowder is shown in Figure 2. As can be seen from the figure, the particles are homogeneous and well defined. The scale bars in the figure correspond to 100 nm, which shows a size of about 15 nm of the nanoparticles. Figure 3 illustrates a TEM micrograph of the ZnO nanoparticles. As can be seen from the figure the powder has a porous agglomerate structure consisting mainly of spherical crystalline particles. The scale bar in the figure corresponds to 20 nm, which shows a particle diameter of about 15–20 nm.

2.2. UV-Vis absorption spectra of the dyes

UV-Vis absorption spectra of the dyes in ethyl alcohol were obtained using a continuous wavelength one-beam spectrophotometer (Thermoline Genesys 6). The wavelength range of absorption spectra analysis extended from

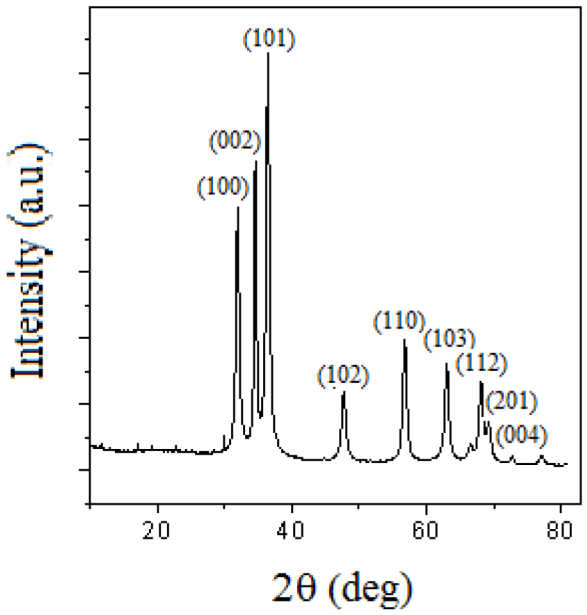

Figure 1. XRD pattern of ZnO powder synthesized at room temperature and pH 12, then dried at 100 °C in air. The peaks correspond to the hexagonal-wurtzite structure in the reference data (JCPDS No. 0036–1451).

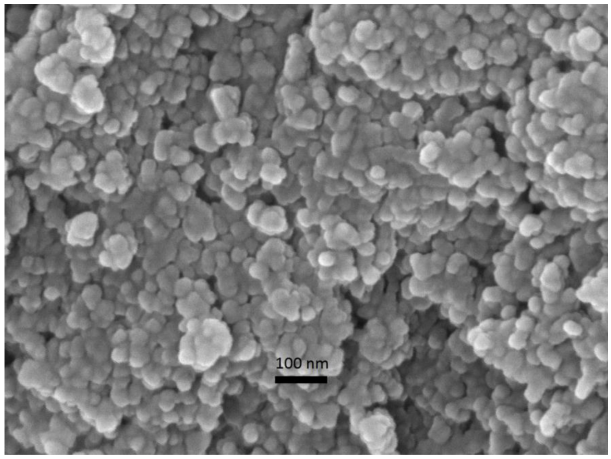

Figure 2. SEM image of the nanostructured ZnO powder synthesized at pH 12. The scale bars correspond to 100 nm.

300 to 800 nm. The following chemical dyes were studied: alcian blue, crystal violet, eosin Y, carbol fuchsin, aniline blue, methyl orange, fast green, and bromophenol. Figures 4 and 5 show the UV-Vis absorption spectra of these dyes. From Figure 4, it can be seen that there is an absorption peak at about 522 nm for eosin Y dye. The absorption spectrum of alcian blue dye shows two peaks at 624 nm and 671 nm. Crystal violet dye has an absorption peak in the visible region at 588 nm. Carbol fuchsin dye exhibits a peak at 552 nm. As can been seen from Figure 5, there are absorption peaks at 362 nm and 444 nm for methyl orange dye, whereas bromophenol dye exhibits an absorption peak at 430 nm. Fast green dye has a peak at 619.8 nm. Finally, aniline blue dye shows a wide peak with a maximum at 624.8 nm.

Eosin Y is a well-known synthetic dye and can be used in many applications. It has a molecular formula of $C_{20}H_8Br_4O_5$ and a molecular weight of 647.89. It is a pink water-soluble acid dye. It was reported that eosin Y displays yellow-green fluorescence [22]. Eosin Y shows an intense absorption peak in the visible region at 522 nm, which corresponds to the maximum absorption peak of the eosin Y monomer. When the ZnO layer was dyed with eosin Y, the spectrum was studied again. Figure 6 shows the UV-Vis spectra of eosin Y dye in ethyl alcohol and eosin Y adsorbed on ZnO film. The absorption spectrum of eosin Y adsorbed on ZnO is obviously wider and very little shifted compared with that dissolved in ethyl alcohol solution. When eosin Y dye was adsorbed on the ZnO film, the peak was observed at 520 nm, which means that an interaction between the dye and the cationic ZnO surface occurred.

2.3. DSSC preparation

FTO conductive glass sheets were cut into pieces of dimensions 0.8 cm × 1.6 cm. The samples were cleaned in a detergent solution using an ultrasonic bath for 15 min, rinsed with water and ethanol, and then dried. The ZnO paste was prepared by adding 0.062 g of ZnO and 0.072 g of polyethylene glycol and then grinding the

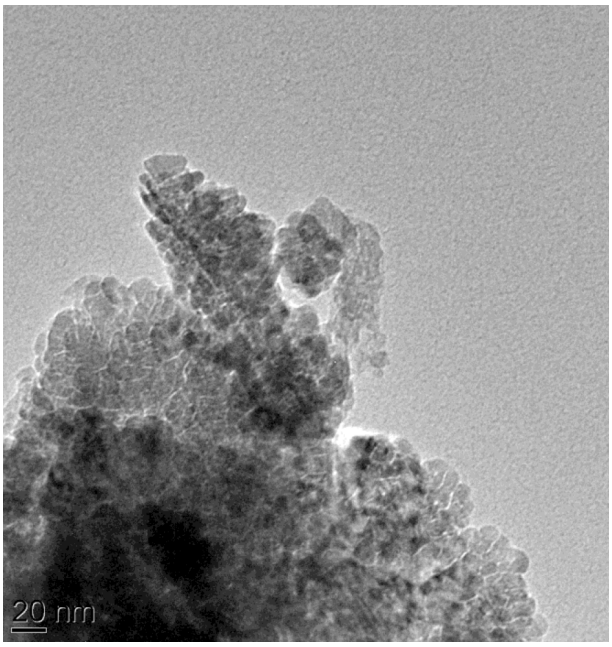

Figure 3. TEM image of the nanostructured ZnO powder synthesized at pH 12 and dried at 100 °C for 12 h. The scale bar corresponds to 20 nm.

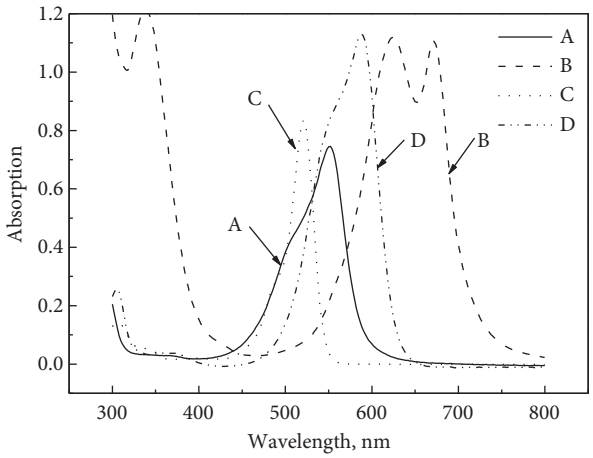

Figure 4. UV-Vis absorption spectra of (A) alcian blue, (B) crystal violet, (C) eosin Y, and (D) carbol fuchsin dyes in ethyl alcohol solution.

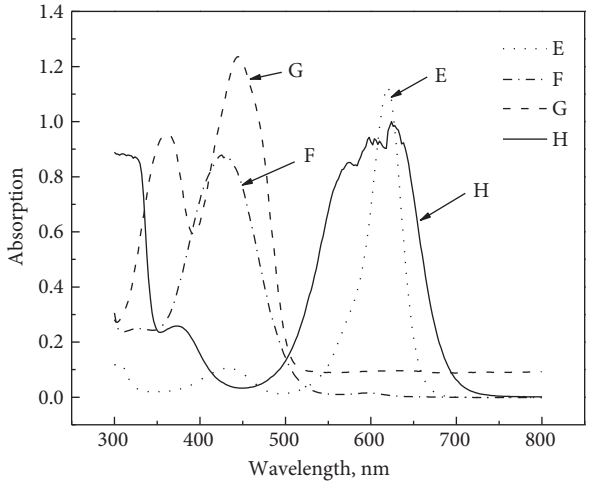

Figure 5. UV-VIS absorption spectra of (E) fast green, (F) bromophenol, (G) methyl orange, and (H) aniline blue dyes in ethyl alcohol solution.

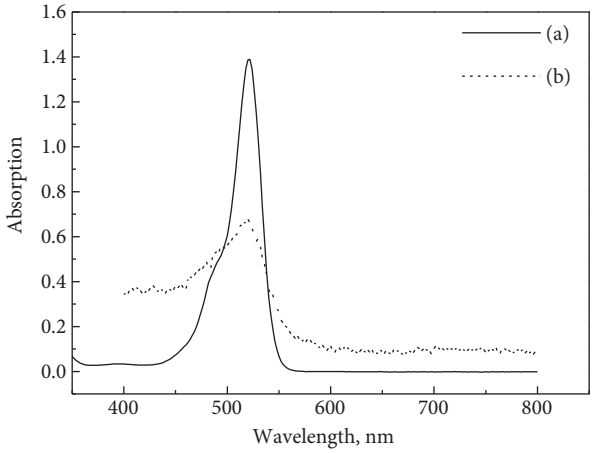

Figure 6. The absorption spectra of (a) eosin Y dye in ethyl alcohol and (b) eosin Y dye adsorbed on ZnO layer.

mixture for 30 min until a homogeneous paste was obtained. The doctor blade technique was used to deposit the nanocrystalline ZnO layers of the active area of 0.25 cm^2 onto the FTO coated glass. To eliminate the solvents, the ZnO layers were placed in an oven at 70 °C for 20 min. Finally, the samples were sintered at 500 °C for 40 min. Samples were cooled to about 70 °C before being placed in dyes for 1 day under dark. The solutions of the dyes were prepared by adding 0.000491 M dye powder to 20 mL of ethyl alcohol. The solutions of the dyes were left for 1 day at room temperature [23]. The dyed ZnO electrode and a sputtered-platinum counter

electrode were assembled to form the DSSC. The redox (I^-/I_3^-) electrolyte solution was sandwiched between the two electrodes. The electrolyte solution consisted of 2 mL of acetonitrile, 0.0944 M propylene carbonate, 0.00499 M LiI, and 0.00049 M I_2.

2.4. Photovoltaic electrical measurements

The current density-voltage ($J-V$) measurements were conducted using an NI USB6251 data acquisition card in combination with the LabVIEW program. These measurements were performed under 100 mW/cm^2 illumination from a high-pressure mercury arc lamp in the dark. Figure 7 shows $J-V$ characteristic curves of the DSSCs sensitized by alcian blue, crystal violet, eosin Y, and carbol fuchsin dyes, whereas Figure 8 illustrates the $J-V$ curves of the cells sensitized by Fast green, bromophenol, methyl orange, and aniline blue dyes. The two figures show the $J-V$ characteristic curves of the DSSCs under illumination as well as in dark conditions. Table 1 presents the parameters of the fabricated cells such as open circuit voltage (V_{oc}), short circuit current density (J_{sc}), fill factor (FF), and conversion efficiency (η). The fill factor is calculated using the following formula:

$$FF = \frac{I_{mp}\,V_{mp}}{I_{sc}\,V_{oc}}, \tag{1}$$

where I_{mp} and V_{mp} are the current and voltage at the maximum power output. The energy conversion efficiency is defined as:

$$\eta = \frac{FF\,I_{sc}\,V_{oc}}{P_{in}}, \tag{2}$$

where P_{in} is the power of incident light.

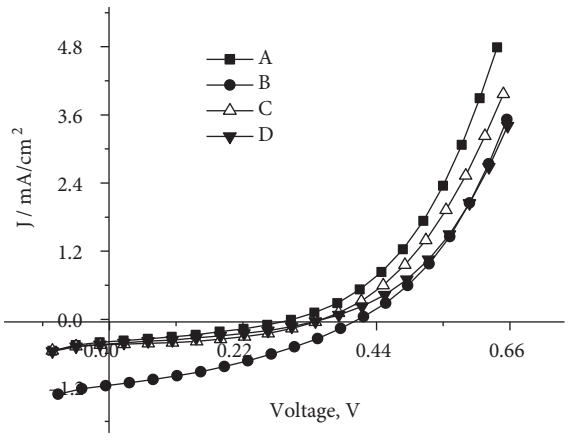

Figure 7. Current density–voltage curves for the DSSCs sensitized by (A) alcian blue, (B) eosin Y, (C) crystal violet, and (D) carbol fuchsin dyes.

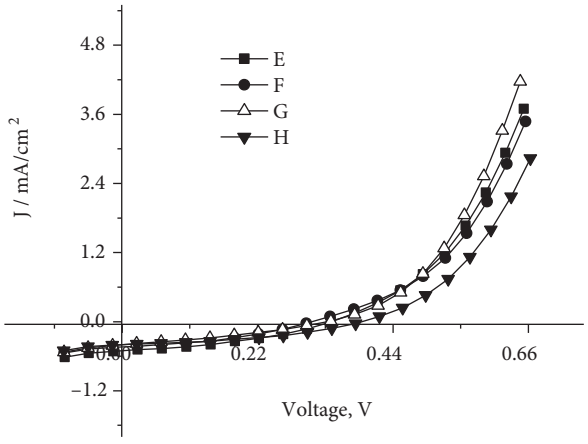

Figure 8. Current density–voltage curves for the DSSCs sensitized by (E) aniline blue, (F) methyl orange, (G) fast green, and (H) bromophenol dyes.

It is clear that the DSSC sensitized with eosin Y dye exhibits the best performance among other cells ($J_{sc} = 1.16$ mA/cm^2, $V_{oc} = 0.408$ V, $FF = 0.32$, and $\eta = 0.15\%$).

Table 1. Photoelectrochemical parameters of the DSSCs sensitized by various chemical dyes.

Chemical dye	λ_{max} (nm)	J_{sc}(mA/cm^2)	V_{oc} (V)	FF (%)	η (%)
Eosin Y	522	1.16	0.408	32	0.15
Alcian blue	626, 672	0.37	0.300	34	0.038
Crystal violet	588	0.61	0.304	31	0.057
Carbol fuchsin	552	0.54	0.345	45	0.080
Fast green	619.8	0.47	0.341	30	0.047
Bromophenol	430	0.48	0.384	38	0.071
Methyl orange	362, 444	0.48	0.302	40	0.058
Aniline blue	624.8	0.48	0.343	42	0.071

3. The influence of the ZnO electrode sintering temperature and thickness

3.1. The effect of sintering temperature

ZnO paste was prepared by dispersing ZnO nanoparticles in polyethylene glycol with a weight ratio of 1:1. After spreading the paste on the FTO coated glass, each layer was sintered at a different temperature (250, 300, 350, 400, 450, 500, and 600 °C) for 40 min. It was reported that ZnO can be sintered between 300 °C and 1000 °C since the melting point of ZnO is 1975 °C [24]. The sintering process was followed by dying the sample with eosin Y, which exhibited the highest efficiency among other dyes. Figure 9 shows the J-V characteristics of the DSSCs under 100 mW/cm^2 illumination. The figure indicates that the cell response is critically dependent on the sintering temperature of the ZnO layer. It is clear that the highest values of V_{oc} and J_{sc} are obtained for the cell sintered at 450 °C. Values of short circuit currents and open circuit voltages of all cells sintered at various temperatures are presented in Table 2.

Table 2. Parameters of the DSSCs sensitized at different temperatures and under 100 mW/cm^2 illumination level.

Temperature (°C)	250	300	350	400	450	500	600
J_{sc}(mA/cm^2)	0.46	0.62	1.14	0.56	1.33	0.60	0.74
V_{oc} (V)	0.380	0.340	0.370	0.380	0.411	0.355	0.360

3.2. Dependence on electrode thickness

To obtain different ZnO film thicknesses, we fixed the amount of polyethylene glycol and changed the weight of ZnO to get different concentrations. Eight different thicknesses in the range of 2.2–9.8 μm were prepared. The thickness of the ZnO layer was measured using a general microscope based on the depth of focus [25]. A sintering temperature of 450 °C was adopted as it corresponds to the highest photoelectrical response. The $J-V$ characteristics of these cells are shown in Figure 10 under 100 mW/cm^2 illumination. The short circuit current density J_{sc} increases with increasing film thickness, with a highest value at 7.5 μm. The highest cell efficiency η is also achieved at this thickness. It should be pointed out that the thickness of ZnO is a significant parameter for the transfer of electrons as well as adsorption of dye. Moreover, it is one of the factors causing the dark current. Therefore, the enhancement of J_{sc} may be attributed to the increased dye absorption by the film. The decrease of J_{sc} at a film thickness of 9.8 μm may be attributed to poor transportation of electrons caused by the thickness of the film. Values of J_{sc} and V_{oc} of all cells are given in Table 3. It was reported that a TiO_2 film of 10 μm in thickness exhibited the best performance with N3 dye [26]. In 2012, the highest

overall power conversion efficiency of 5.61% was obtained with a 26-μm-thick ZnO photoelectrode sensitized by N719 dye [27].

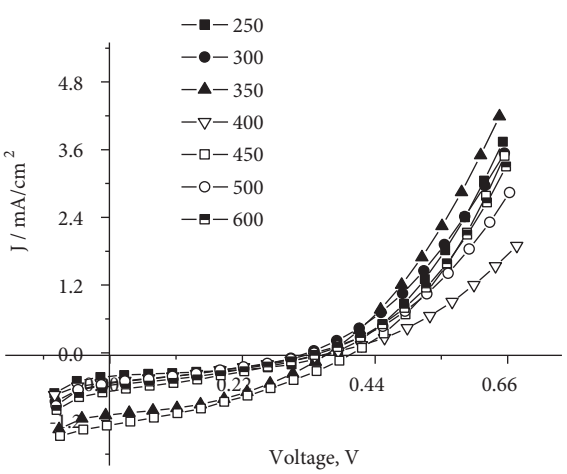

Figure 9. Current density–voltage characteristics of ZnO-DSSCs with photoelectrodes sintered at different temperatures (°C).

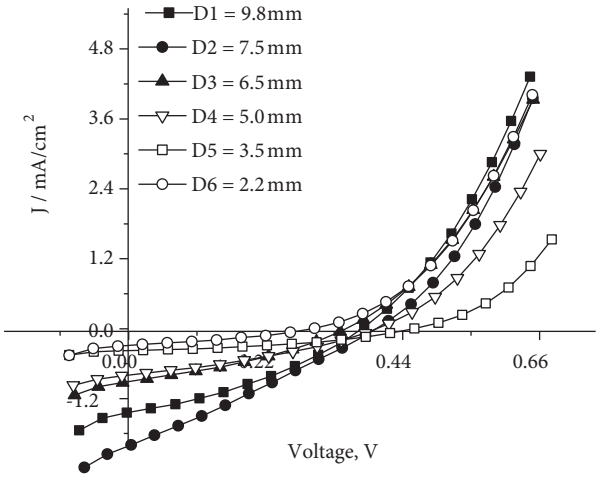

Figure 10. Current density–voltage curves for the DSSCs prepared at different thicknesses of the ZnO layer.

Table 3. Parameters of the DSSCs sensitized at different thicknesses and under 100 mW/cm^2 illumination level.

2.2	3.5	5	6.5	7.5	9.8	Thickness (μm)
0.38	0.82	0.31	0.96	2.11	1.50	J_{sc} (mA/cm^2)
0.492	0.419	0.328	0.364	0.411	0.387	V_{oc} (V)

4. Conclusions

In this work, DSSCs were assembled using eight synthetic dyes as sensitizers for a nanocrystalline ZnO photoelectrode. The ZnO nanoparticles, with crystallite mean value of 12 nm as indicated from XRD data, were synthesized at pH 12. SEM pictures and TEM micrographs of the ZnO powder revealed homogeneous and well-defined nanoparticles with a size of about 15 nm and showed that the powder had a porous agglomerate structure consisting mainly of spherical crystalline particles of about 15–20 nm in diameter, respectively.

Photovoltaic parameters such as short circuit current density J_{sc}, open circuit voltage V_{oc}, fill factor FF, and overall conversion efficiency η for the fabricated DSSCs were determined under 100 mW/cm^2 illumination and then compared. It was found that the DSSC dyed with eosin Y showed the best performance. We also found that the performance of this DSSC increases with increasing semiconductor electrode sintering temperature, with highest performance at 450 °C. It was found that the thickness of the semiconductor electrode is important for better cell performance, with highest response at an electrode thickness of 7.5 μm.

References

[1] O'Regan, B.; Grätzel, M. *Nature* **1991**, *353*, 737–740.

[2] Hagfeldt, A.; Grätzel, M. *Acc. Chem. Res.* **2000**, *33*, 269–277.

[3] Chiba, Y.; Islam, A.; Watanabe, Y.; Komiya, R.; Koide, N.; Han, L. *Jpn. J. Appl. Phys.* **2006**, *45*, 638–640.

[4] Dai, Q.; Rabani, J. *J. Photochem. Photobiol. A* **2002**, *148*, 17–24.

[5] Espinosa, R.; Zumeta, I.; Santana, J. L.; Martınez-Luzardo, F.; Docteur, S.; Vigil, E. *Sol. Energy. Mat. Sol. C* **2005**, *85*, 359–369.

[6] Zhou, H.; Wu, L.; Gao, Y.; Ma, T. *J. Photoch. Photobio. A* **2011**, *219*, 188–194.

[7] Chen, H.; Duan, Z.; Lu, Y.; Pasquier, A. *J. Electron. Mater.* **2009**, *38*, 1612–1617.

[8] Hamann, T.; Martinson, A.; Elam, J.; Pellin, M.; Hupp, J. *Adv. Mater.* **2008**, *20*, 1560–1564.

[9] Longyue, Z.; Songyuan, D.; Weiweir, X.; Kongjia, W. *Plasma Sci. Technol.* **2006**, *8*, 172–175.

[10] Batniji, A.; Morjan, R.; Abdel-Latif, M.; El-Agez, T.; Taya, S.; El-Ghamri, H. *Turk. J. Phys.* **2014**, *38*, 86–90.

[11] El-Agez, T.; Taya, S.; ElRefi, K.; Abdel-Latif, M. *Opt. Appl.* **2014**, *44*, 345–351.

[12] Taya, S.; El-Agez, T.; Abdel-Latif, M.; El-Ghamri, H.; Batniji, A.; El-Sheikh, I. *International Journal of Renewable Energy Research* **2014**, *4*, 384–388.

[13] Taya, S.; El-Ghamri, H.; El-Agez, T.; Abdel-Latif, M.; Batniji, A. *British Journal of Applied Science & Technology* **2015**, *5*, 380–386.

[14] El-Ghamri, H.; El-Agez, T.; Taya, S.; Abdel-Latif, M.; Batniji, A. *Materials Science-Poland* **2015**, *35*, 547–554.

[15] El-Agez, T.; El Tayyan, A.; Al-Kahlout, A.; Taya, S.; Abdel-Latif, M. *International Journal of Materials and Chemistry* **2012**, *2*, 105–110.

[16] Hongsith, N.; Sae-kang, C.; Mangkorntong, P.; Mangkorntong, N.; Choopun, S. *CMU J. Nat. Sci.* **2008**, 7, 171–176.

[17] Kolemen, S.; Bozdemir, O.; Cakmak, Y.; Barin, G.; Erten-Ela, S.; Marszalek, M.; Yum, J.; Zakeeruddin, S.; Nazeeruddin, M.; Grätzel, M. et al. *Chem. Sci.* **2011**, 2, 949–954.

[18] Cakir, A.; Erten-Ela, S. *Adv. Powder Technol.* **2012**, 23, 655–660.

[19] Rani, S.; Suri, P.; Shishodia, P. K.; Mehra, R. M. *Sol. Energy Mater. Sol. Cells* **2008**, *29*, 1639–1645.

[20] Al-Kahlout, A. *Thin Solid Films* **2012**, *520*, 1814–1820.

[21] Aghababazadeh, R.; Mazinani, B.; Mirhabibi, A.; Tamizifar, M. *J. Phys. Conf. Ser.* **2006**, *26*, 312–320.

[22] Perez, M.; Torrades, F.; Domenech, X.; Peral, J. *Water Res.* **2002**, *36*, 2703–2710.

[23] Yamazaki, E.; Murayama, M.; Nishikawa, N.; Hashimoto, N.; Shoyama, M.; Kurita, O. *Sol. Energy* **2007**, *81*, 512–516.

[24] Gray, T. *J. Am. Ceram. Soc.* **1954**, *37*, 534–538.

[25] Liu, J.; Tian, C.; Wang, Z.; Lin, J. *Eurasian Journal of Analytical Chemistry* **2007**, *2*, 12–20.

[26] Baglio, V.; Girolamo, M.; Antonucci, V.; Aricò, A. *Int. J. Electrochem. Sci.* **2011**, 6, 3375–3384.

[27] Chang, W.; Lee, C.; Yu, W.; Lin, C. *Nanoscale Res. Lett.* **2012**, *7*, 688–697.